

A New Perspective on Material Classification and Ink Identification

Rakesh Shiradkar[†], Li Shen[‡], George Landon[§], Sim Heng Ong[†] and Ping Tan[†]

[†]National University of Singapore [‡]Institute for Infocomm Research [§]Eastern Kentucky University

Abstract

The surface bi-directional reflectance distribution function (BRDF) can be used to distinguish different materials. The BRDFs of many real materials are near isotropic and can be approximated well by a 2D function. When the camera principal axis is coincident with the surface normal of the material sample, the captured BRDF slice is nearly 1D, which suffers from significant information loss. Thus, improvement in classification performance can be achieved by simply setting the camera at a slanted view to capture a larger portion of the BRDF domain. We further use a handheld flashlight camera to capture a 1D BRDF slice for material classification. This 1D slice captures important reflectance properties such as specular reflection and retro-reflectance. We apply these results on ink classification, which can be used in forensics and analyzing historical manuscripts. For the first time, we show that most of the inks on the market can be well distinguished by their reflectance properties.

1. Introduction

Different materials can be distinguished by examining their reflectance properties encoded in the bi-directional reflectance distribution function (BRDF) [20]. Conventionally, BRDFs are represented as 4D functions of the incident and reflected lighting direction \mathbf{l} and \mathbf{v} respectively. Therefore, previous material classification methods, such as [20], capture a ‘2D BRDF slice’ by fixing the camera and changing the incident lighting directions.

It is well known the 4D BRDF representation is redundant. For example, factorization techniques [10, 13] represent an arbitrary BRDF as the sum of products of 2D functions for efficient storage and rendering. Under appropriate parameterization [16, 19], an isotropic BRDF can be well approximated as a 2D function of the ‘half-angle’, θ_h , and the ‘difference angle’, θ_d . (See Figure 1 for the definition of these angles.) Many real materials are isotropic or near isotropic. Therefore, many BRDFs are near 2D.

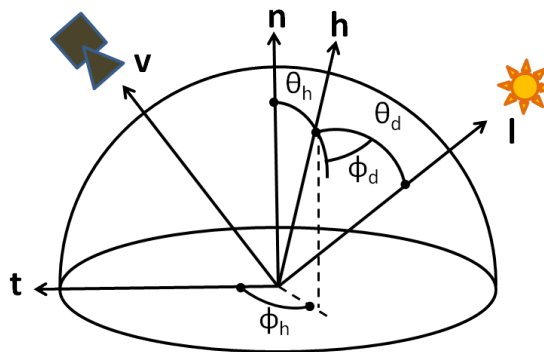


Figure 1: The half-vector parameterization of BRDF. The incident and reflected lighting directions \mathbf{l} and \mathbf{v} provide a 4D parameterization of a BRDF function. The BRDFs of many isotropic materials can be well approximated as a 2D function of the half-angle θ_h and the difference angle θ_d .

In previous material classification works [20, 8, 9], the camera directly faces the sample material to provide the most fronto-parallel image for better image resolution. However, this causes a degeneration where the ‘half-angle’ θ_h is always equal to the ‘difference angle’ θ_d , because the surface normal \mathbf{n} is coincident with the viewing direction \mathbf{v} . In other words, even if the sampled incident lighting directions \mathbf{l} cover the whole upper hemisphere, we effectively only capture a 1D BRDF slice. This degeneration causes significant information loss. In fact, as we will see in later sections, both Fresnel effects and retro-reflectance cannot be effectively captured under this degenerate setting.

The remedy is strikingly simple. We only need to set the camera to a slanted angle. Note that this setting is rare, since the fronto-parallel view provides better uniform resolution of the material sample. From the slanted perspective, we can capture a bigger portion of the 2D BRDF domain. In our experiments, we find this simple change improves the overall accuracy from 78% to 85% for classification over 55 different inks.

We then adopt a handheld flashlight camera for 1D

BRDF slice capture. This setting allows us to obtain a 1D BRDF slice where the ‘difference angle’ θ_d is fixed at zero, but θ_h can change from 0 to $\pi/2$. This slice can capture distinctive reflectance properties such as specular reflection (when θ_h is small) and retro-reflectance (when θ_h is large). It achieves a reasonable classification accuracy with fewer input images and more flexible data capture comparing to the conventional setting [20, 8, 9].

We apply these results to the ink strokes classification problem, which has extensive applications in forensics for analyzing questionable documents and historical manuscripts [12, 18]. Spectral analysis based techniques such as spectroscopy and infrared reflectography [5, 7] are extensively used to classify different inks according to their light absorption at different wavelengths. These methods usually require special devices by which the optical properties of the pigments are examined under illumination beyond the visible spectrum. Our contributions include investigating and demonstrating that the BRDFs of major types of inks in the market as well as manuscript inks can often be distinguished by analyzing their BRDF slices. Our method provides a low-cost solution for ink classification. To the best of our knowledge, this is the first work that applies material classification to document analysis.

2. Related Work

Reflectance-based Material classification Classifying materials based on reflectance is a relatively less explored area. Wang et al. [20] propose a method of material classification using ‘2D BRDF slices’. They capture a ‘2D BRDF slice’ by capturing images with a fixed camera and varying illumination. They then fit hemispherical harmonics to the observations and use the coefficients as a basis for classification. Jehle et al. [8] and Gu and Liu[9] further studied the optimal illumination condition to enhance the separation. We study the sample distribution in the BRDF domain and prove that a slanted camera can significantly improve classification accuracy. We further develop a method to capture a 1D BRDF slice with a handheld flashlight camera.

Ink Classification Documents and manuscripts are analyzed for their authenticity and dating by determining the type of ink material. The existing methods for such an analysis can be broadly characterized into destructive and non-destructive types, the latter being preferred. In this paper, we focus on the non-destructive types. Most non-destructive methods such as spectroscopy and reflectography [5, 7] use illumination beyond the visible spectrum. Alternatively, image processing based methods offer cost effective and non-destructive solutions by computing models and analyzing ink properties in the visible domain. Chakravarthy et al. [3] showed that statistical properties

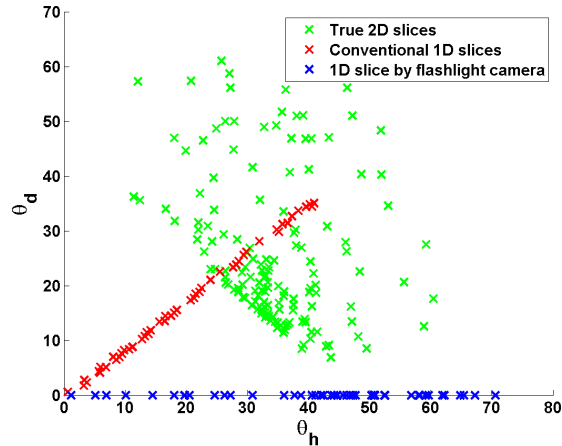


Figure 2: The sample distribution in the θ_h - θ_d space. The conventional setting (i.e. $\mathbf{v} \approx \mathbf{n}$) collects red samples along a straight line. By simply setting the camera at a slanted angle, we collect the green samples spanning a larger range of the BRDF domain. The blue samples are collected by a handheld flashlight camera.

such as saturation histograms in HSV color space can differentiate liquid inks and viscous inks. This color analysis based method cannot distinguish inks of similar color. Kokla et al. [11] propose a method to distinguish inks by studying statistical properties of the ink intensities in visible and infrared light. However, the accuracy reported is not very high. Licata et al. [12] propose a near IR based method for distinguishing and restoring inks in historical manuscripts. Hu et al. [4] provide a survey of ink segmentation methods used in forensics. None of the above methods in ink segmentation have studied the reflectance properties of inks for segmentation. A recent work by Berger [1] describes an ink segmentation method based on color deconvolution. This method can distinguish inks of similar color based on intrinsic differences in the ink shades. However, it cannot deal with common black inks with almost constant shade. Our method is based on the reflectance properties of manuscript inks, which can identify different inks of similar color. Our method outperforms Berger’s method[1].

3. Dimensionality of BRDF Slices

BRDFs of real materials exhibit strong symmetry and redundancy such as isotropy, reciprocity, half-vector symmetry, etc. Thus, the dimension of the BRDF domain can be often safely reduced. As shown in Figure 1, a BRDF can be parameterized as a 4D function $f(\theta_h, \phi_h, \theta_d, \phi_d)$. There is strong evidence that many BRDFs can be well approximated by a 2D function $f(\theta_h, \theta_d)$. Specifically, the isotropy reduces the BRDF domain to $(\theta_h, \theta_d, \phi_d)$. The half-vector

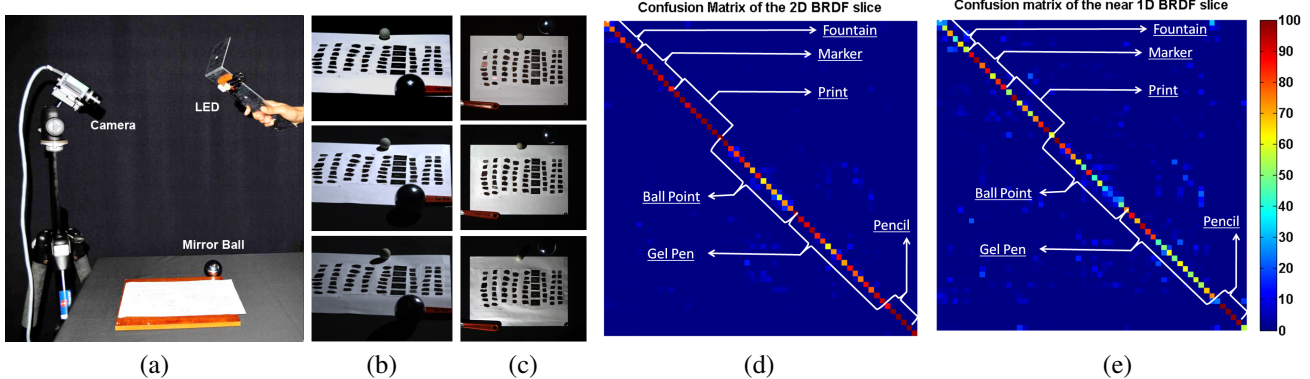


Figure 3: Experiment on ink classification based on true 2D BRDF slices and near 1D BRDF slices. a) Acquisition setup for true 2D BRDF data. b) and c) Input images for the true 2D BRDF slices and near 1D BRDF slices respectively. d) Confusion matrix for ink classification with true 2D BRDF slices. It achieves average accuracy of 85% over 55 inks. e) Confusion matrix result with near 1D BRDF slices. The average accuracy is 78%.

symmetry[23], which suggests the BRDF is unchanged by a rotation of \mathbf{l} and \mathbf{v} around the bisector \mathbf{h} , further reduces the BRDF domain to (θ_h, θ_d) . This 2D representation is empirically verified in [15] with the MERL BRDF database [14] and recently applied for photometric stereo [17].

In the following, we analyze the material classification problem with this 2D BRDF approximation. In previous methods [20, 9], the camera is usually oriented in a way such that $\mathbf{v} \approx \mathbf{n}$. In this case, the angles $\theta_h = \arccos(\mathbf{h}^\top \mathbf{n})$ is approximately equal to $\theta_d = \arccos(\mathbf{h}^\top \mathbf{v})$. Effectively, only a 1D slice of the BRDF can be captured no matter how many lighting samples are collected from the upper hemisphere. Furthermore, the range of θ_d and θ_h is restricted to $[0, \pi/4]$. This problem is clearly demonstrated in Figure 2. We move a LED light on the upper hemisphere of a planar sample. Each red cross indicates an observation captured by a camera facing directly to the sample. All these sample points are near a line segment in the θ_h - θ_d space. This set of samples does not capture some important phenomena such as retro-reflectance¹ and Fresnel effects² that make certain materials distinctive. Typically, the retro-reflectance is stronger when $\theta_d = 0$ and $\theta_h > \pi/3$. The Fresnel effect is most significant when $\theta_d > \pi/3$.

To achieve improved ranges of θ_d and θ_h , we can simply orient the camera to a slightly slanted direction. Under similar motion of the LED lights, we can collect samples shown in green in Figure 2. These samples cover a larger portion of the BRDF domain. Naturally, they encode more reflectance properties and will make the material classification problem simpler.

¹Retro-reflectance is the phenomenon that light is reflected back towards the incident direction.

²Fresnel effects explain the increased specular reflection at the grazing angle.

4. Consequence on Material Classification

To verify our analysis, we collect 55 different pens of various types (water soluble, gel, ball point, permanent marker) and from different manufacturers (Pilot, Zebra, Uni-ball, Staedtler, Pentel, Faber-Castell, Parker, etc.). We capture multiple images of a flat document containing different ink strokes under varying illumination directions. We collect two sets of images, one set for a slanted camera (i.e. a true 2D BRDF slice), one set for the camera facing directly to the document (i.e. a near 1D BRDF slice because of $\mathbf{v} \approx \mathbf{n}$). The data capture setup and some sample images are provided in Figure 3 (a), (b) and (c). All the lighting intensities and directions are recorded with calibration objects. The incident lighting direction is densely sampled over the upper hemisphere defined by the document surface normal. From the recorded image radiance I and calibrated lighting information, we can get a sample of the 2D BRDF from each pixel of each image according to the following equation.

$$f(\theta_d, \theta_h) = I(\mathbf{x}) / (\mathbf{n} \cdot \mathbf{l}). \quad (1)$$

We then take this recovered BRDF as a distinguishing feature for material classification. In our images, each ink often covers 4000 pixels. We randomly select 1000 pixels for each ink to train a standard support vector machine (SVM) classifier [2]. The classifier is then applied to the remaining pixels for evaluation. The classification results (in terms of a confusion matrix) with the true 2D BRDF slice and the near 1D BRDF slice are shown in Figures 3 (d) and (e) respectively. Almost all the inks are successfully classified when the true 2D BRDF slices are used. The average classification accuracy is 85% for the 55 inks. This high accuracy clearly demonstrates that BRDFs provide a strong cue to identify different inks. However, when the near 1D BRDF slices are used, the performance is dropped

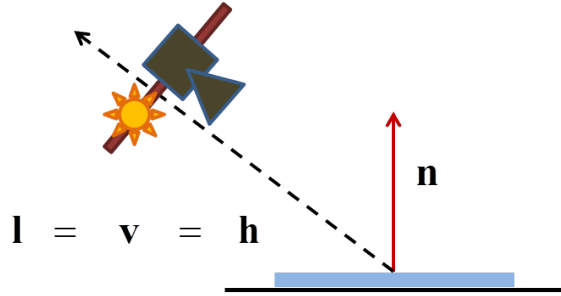


Figure 4: Schematic diagram showing the handheld flashlight camera arrangement.

to 78%. This demonstrates the importance of selecting the right BRDF domain sampling strategy. When the samples cover a larger range, more reflectance properties can be captured and the classification performance will be better.

5. A Handheld Capture Method

To allow flexible data capture, we propose to use a handheld flashlight camera to capture BRDF slices for material classification. When images are captured with a light attached to the camera as shown in Figure 4, the incident and outgoing lighting directions are coincident, i.e. $\mathbf{l} = \mathbf{v}$. Thus, the half-vector \mathbf{h} overlaps with \mathbf{v} , and θ_d is always 0. By moving the camera around, we can capture images with θ_h varying over the range of $[0, \pi/2]$. This simple setting allows us to capture some important reflectance properties. Firstly, specular reflectance highly depends on θ_h [16]. Since our method covers the full dynamic range of θ_h , it faithfully captures the characteristics of specular reflections, e.g. the strength and extent of specular lobes. Secondly, retro-reflectance often becomes stronger when $\theta_d = 0$ and $\theta_h > \pi/3$. Therefore, our method can also capture retro-reflectance to help distinguish different materials. Lastly, by fixing θ_d , we cannot capture any Fresnel effects. A possible solution is to attach multiple lights to the camera, each with a different distance to the camera. By turning these lights on and off during image recording, we can capture Fresnel effects. However, this setting is more complicated and we found empirically our flashlight camera setting works well for ink identification.

To verify the performance of this handheld system, we apply it to the flat document sample with the 55 inks. Figure 5 (a) shows the confusion matrix based on this handheld device. The average classification accuracy is 71%. Though the classification accuracy is reduced comparing to the true 2D BRDF slices, this performance is still good for classification of 55 inks. Typically, an ink stroke consists of several hundreds of pixels. We empirically find this classification accuracy is good enough to detect document forgery. The reduced accuracy is partly because of the imprecision

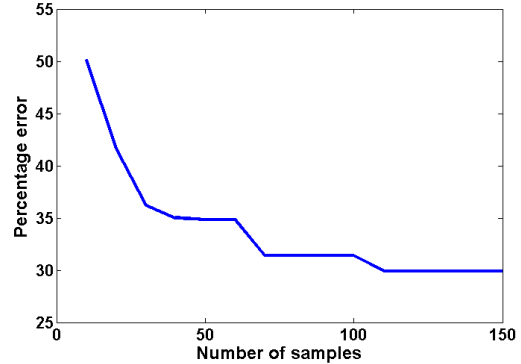


Figure 6: Classification error rate of the conventional data capture setting where the camera faces directly to the sample.

in registration when capturing with a handheld device. We can observe that performance for Marker, Prints, Pencil and Gel pens have quite high accuracy, while the performance for Ball Point pens and fountain inks have quite low accuracy.

5.1. Distinctive Intervals

To further understand which interval of θ_h is more informative for material classification, we cut the 1D BRDF slices into multiple overlapping segments. We perform similar SVM based classification based on each of these segments. The result is summarized in Figure 5 (b). We observe that: 1) The classification accuracy is highest in the range of 1 – 25 degrees and gradually falls after that and slightly rises in the range of (65 – 85) degrees. These two ranges correspond to the specular and retro-reflectance phenomena respectively. It confirms our design choice of using a flashlight camera. 2) classification accuracy using the full 1D BRDF slice, 71%, is greater than using any individual range, $< 60\%$. This suggests a full sampling of θ_h in the range $[0, \pi/2]$ is useful.

5.2. Number of Images

We further investigate what is the appropriate number of input images for this method. We show its performance against the number of randomly sampled images in Figure 5 (c). Here, samples are randomly selected over the range of θ_h . The overall classification error curve takes a sharp turn at samples 10 to 20 and gradually falls after that. The classification error remains almost constant after the number of samples reaches 30. Therefore, we select around 30 samples for later experiments. For a comparison, we provide a similar error curve for the conventional data capture setting in Figure 6. It will take over 100 images to reach similar classification accuracy.

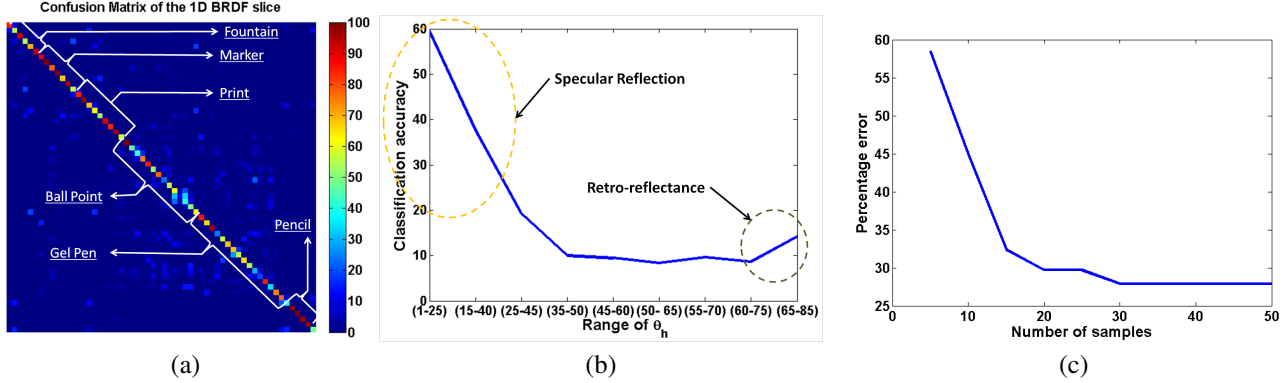


Figure 5: a) Confusion table showing the separability of the 55 inks using the proposed handheld flashlight camera setting; b) Sensitivity of θ_h ; c) Analyzing the number of samples vs. classification performance.

6. Ink Segmentation on Curved Documents

In this section, we extend the handheld system to work on a general curved document. The 3D document shape is reconstructed to facilitate image registration and 1D BRDF slice estimation. We then apply a clustering method to group pixels with similar BRDF slices together for ink segmentation. Note, we do not seek to identify the type of ink. We only estimate if two pixels have the same ink or not, which is useful for forensics.

3D Reconstruction: The surfaces of documents are often curved. We need a precise 3D reconstruction for image registration so that we can obtain multiple observations for a surface point on the document. We apply the structure-from-motion package VisualSFM [21] to perform 3D reconstruction of the input images. This 3D reconstruction provides the camera locations and a set of sparse 3D points on the document surface. Since the light source is attached to the camera, we obtain the location of the light source directly from this 3D reconstruction.

Surface Fitting: The reconstructed 3D point cloud is often sparse. We fit a parametric surface to the sparse point cloud to recover the 3D shape of the surface. Following the work of Yamashita et al. [22], we make use of Non Uniform Rational B-Spline (NURBS) to fit a smooth parametric surface. This 3D surface also provides an accurate estimation of the normal direction \mathbf{n} at every point.

Image Registration: Given the 3D surface, we can determine the 3D location of each pixel by intersecting a ray from this pixel on the reference image with the 3D surface. By reprojecting this 3D point back on to the other images, we can obtain pixel correspondence among images captured from different viewpoints. We take the view where the document is most fronto-parallel to the camera as the reference view. We then project the 3D position of each of its pixels to all the other images to collect multiple observations of each pixel.

BRDF Slice Estimation: We have collected multiple observations of each pixel as observed in the reference view. Further, we know its surface normal direction from the NURBS surface fit, and the lighting directions from the camera positions. Thus, we can recover a 1D BRDF slice for each pixel from Equation 1.

Ink Identification: The estimated BRDF profiles will be used as a discriminative feature for ink classification. We compare the BRDF slices of different points. Noting that θ_h varies in the range 0 to $\pi/2$, we sample this interval to 30 bins, and calculate the average BRDF value in each bin for every pixel. The BRDF slices form a discriminative feature for each ink. We can differentiate the inks using clustering techniques by grouping the pixels according to their associated BRDF slices. This will allow us to tell if the inks at some given pixels on a document are different or not. In our experiments, we apply the affinity propagation [6] for clustering.

7. Experiments

7.1. Ink Classification

In Figure 7, we examine the SVM based ink classification on a flat document with some representative inks. As shown in Figure 7(a), a flat document contains horizontal strokes and text written with 12 different inks of black color. The horizontal stroke and the text written beside belong to the same ink type. Pixels on the horizontal strokes are used for training and pixels on the texts are used for testing. The 12 inks are selected from the five major types of inks: pencils (Pencil1, Pencil2), fountain pen inks (Pilot, Stabilo), ballpoint inks (Ball OM, Ball JS, Zebra), mark pen ink (Sharpie, Perm Ptl, Perm Zig), and gel-pen inks (EngerGel, Jimmie).

The classification results are shown as an image in Figure 7(b). We also show the zoomed-in classification results of the inks of the best and worst performance. In Fig-

ure 7(c), we evaluate the separability on these 12 inks in the form of a confusion table. We observe that the carbon ink (Pencil1, Pencil2) and the markers (Perm Ptl, Sharpie) have higher classification accuracy above other inks. The gel pen inks and ballpoint inks have less accuracy but these inks have more confusion among themselves for classification. This observation is consistent the result on 55 inks presented in Figure 3.

We must also note that all the inks are black in color and there are almost negligible variations in their shades. Bearing this fact, the classification result demonstrates that BRDF profiles are promising discriminative features for identifying different inks.

7.2. Ink Segmentation

We further evaluate the ink segmentation on both flat and curved documents. Figure 8 shows the recovered point cloud and the 3D surface of the document from multiple view images. Figure 9 shows our segmentation results, where (a), (b), and (c) are the input image, segmentation result, and ground truth segmentation. As can be seen, the proposed method can correctly group pixels of the same ink in most of the regions. For the example in the top row, we have a curved document containing different inks (Fountain, Zebra, Perm Zig) of black color. The three inks are successfully identified by the proposed method. For the second example, we have a printed book page with 5 different inks (Sharpie, Omni, Pilot, Fountain, EnerGel). We observe the confusion of EnerGel, a gel ink, with Fountain ink. Liquid inks tend to get absorbed in the paper, which leads to the confusion in identification. For the example of cross lines, we have lines with different inks (Fountain, Ball OM, Zebra, Stabilo) intersecting each other. The strokes appear very similar to each other in their color. Our method can differentiate Fountain, Stabilo and Zebra easily, while is confused on Ball OM and Zebra, which are ball point pens, in some regions. As we have observed previously, that ball point pens tend to have confusion amongst themselves. In the last row of Figure 9, we show an interesting example of a forged check. Using the proposed method, we are able to identify different inks and the attempted forgery.

7.3. Comparison

In Figure 10, we compare with Berger’s work [1] which separates inks based on color analysis. Here strokes of the same orientation have the same ink. In Figure 10(a), the inks have slightly different colors, so that both methods work well. However, for the examples in (b-d) where the inks are black with almost no difference in their shades, Berger’s method fails while our method can correctly distinguish them.

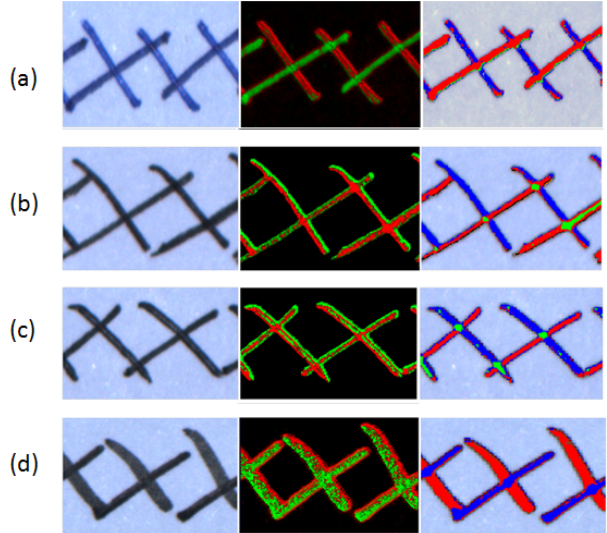


Figure 10: Comparison with Berger’s work [1]. Left: input image. Middle: Bergers result. Right: our result.

8. Conclusions

We analyzed the sampling in the BRDF domain for reflectance based material classification methods and concluded that earlier methods suffer from significant degeneration because they only capture a near 1D BRDF slice. A significant improvement in classification accuracy can be achieved by simply setting the camera to a slanted view. We further propose a flexible method with a handheld flashlight camera, which captures a 1D BRDF slice that encodes distinctive reflectance features such as specular reflection and retro-reflectance. We empirically found this flexible method works as well as previous methods while it requires much fewer images and allows flexible data capture.

In terms of ink identification, we investigated the BRDFs of major types of inks in the market, and showed that the manuscript inks can be successfully identified by the BRDF slices. We have demonstrated the application of our algorithm on flat documents, general curved document, and a realistic case of a fraudulent check. Our method fails to distinguish inks when they have similar reflectance properties. This can happen when the inks are similar in their compositions. Some possible ways to increase the robustness of our method is to consider additional features besides reflectance such as stroke shape, pressure, velocity of the pen tip. We leave this for future work.

Acknowledgements

This material is based upon work supported by the National Science Foundation under Grant No. IIS-1008285. Ping Tan is partially supported by the ASTAR PSF project

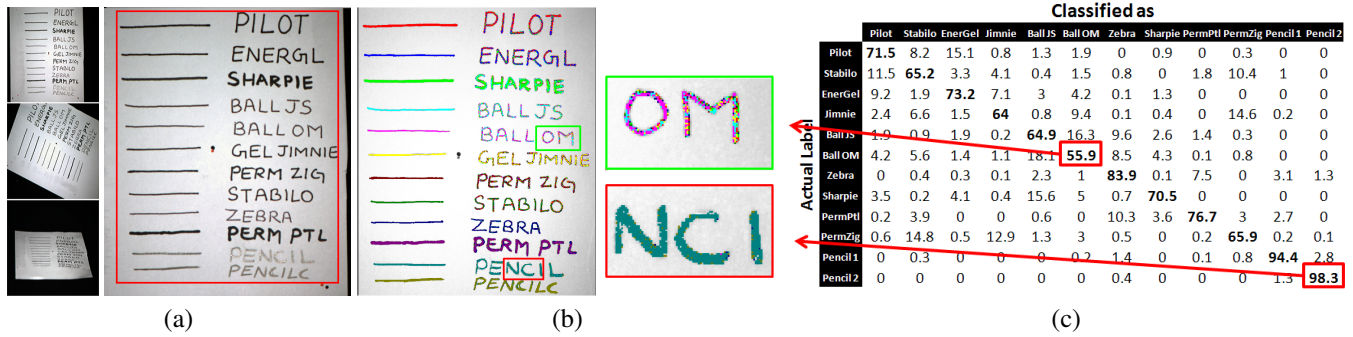


Figure 7: a) Sample images of the ink strokes under different viewpoints, and selected portion of ink strokes; b) Classification of ink strokes by an SVM classifier, with zoomed in results; c) Confusion matrix for classification performance.

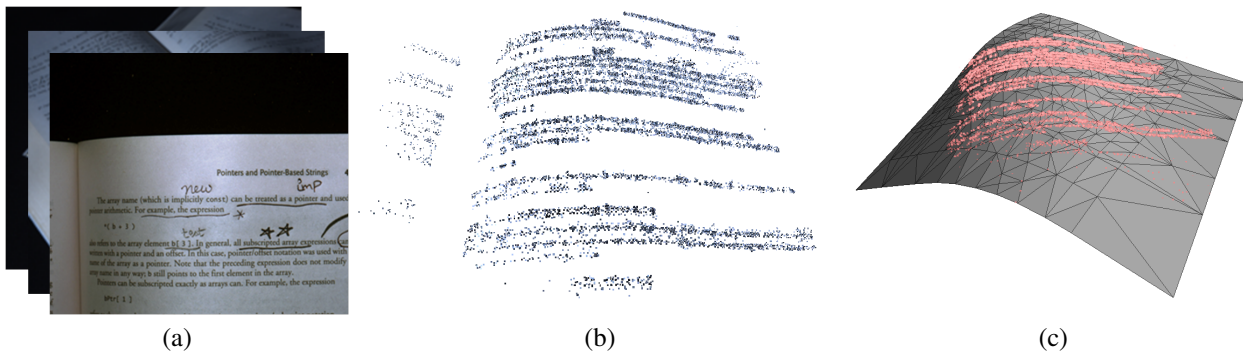
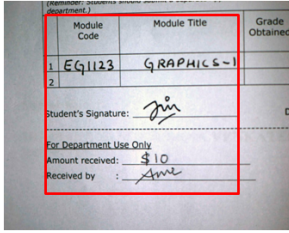


Figure 8: 3D reconstruction of the document surface. a) Multiple images of the document captured using the handheld device; b) Reconstructed sparse point cloud; c) NURBS surface fit through the point cloud.

R-263-000-698-305.

References

- [1] C. E. H. Berger. Objective ink color comparison through image processing and machine learning. *Science and Justice : Journal of the Forensic Science Society*, 53(1):55–59, 2013.
- [2] E. Caputo, B. Hayman and P. Mallikarjuna. Class-specific material categorisation. In *Proc. ICCV*, pages 1597–1604, 2005.
- [3] B. Chakravarthy and H. Dasari. Classification of liquid and viscous inks using hsv colour space. In *Proc. of Intl. Conf. on Doc. Analysis and Recognition*, pages 660–664, 2005.
- [4] H. S. Chen, H. H. Meng, and K. C. Cheng. A survey of methods used for the identification and characterization of inks. *Forensic Science Journal*, 2002.
- [5] B. E. Fau and R. B. Dyer. Fourier transform hyperspectral visible imaging and the nondestructive analysis of potentially fraudulent documents. *Applied Spectroscopy*, 60(3):833–840, 2006.
- [6] B. J. Frey and D. Dueck. Clustering by passing messages between data points. *Science*, 315:972–977, 2007.
- [7] J. C. Harsanyi and C. I. Chang. Hyperspectral image classification and dimensionality reduction: An orthogonal subspace projection approach. *IEEE Trans. on Geoscience and Remote Sensing*, 32(4):779–785, 1994.
- [8] M. Jehle, C. Sommer, and B. Jhne. Learning of optical illumination for material classification. *Pattern Recognition*, 6376:563–572, 2010.
- [9] G. Jinwei and C. Liu. Discriminative illumination: Per-pixel classification of raw materials based on optimal projections of spectral brdf. In *Proc. CVPR*, 2012.
- [10] J. Kautz and M. D. McCool. Interactive rendering with arbitrary brdfs using separable approximations. In *Proc. ACM SIGGRAPH*, 1999.
- [11] V. Kokla, A. Psarrou, and V. Konstantinou. Ink recognition based on statistical classification methods. In *Proc. of Intl. Conf. on Doc. Image Analysis for Libraries*, pages 254–264, 2006.
- [12] A. Licata, A. Psarrou, and V. Kokla. Unsupervised ink type recognition in ancient manuscripts. In *Proc. ICCV, Workshops*, pages 955–961, 2009.
- [13] M. D. McCool, J. Ang, and A. Ahmad. Homomorphic factorization of brdfs for high-performance rendering. In *Proc. ACM SIGGRAPH*, 2001.
- [14] L. Mcmillan, A. Smith, and W. Matusik. A data-driven reflectance model. In *Proc. ACM SIGGRAPH*, 2003.
- [15] F. Romeiro, Y. Vasilyev, and T. Zickler. Passive reflectometry. In *Proc. ECCV*, 2008.



Module Code	Module Title	Grade Obtained
1 EQ1123	GRAPHICS-1	
2		

Student's Signature: Jim

For Department Use Only

Amount received: \$10

Received by: Jim

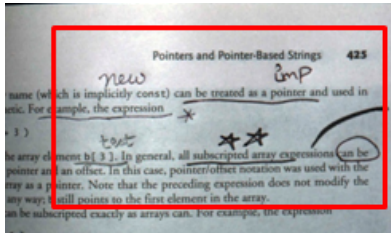
Module Code	Module Title	Grade Obtained
1 EQ1123	GRAPHICS-1	
2		

Student's Signature: Jim

For Department Use Only

Amount received: \$10

Received by: Jim



Pointers and Pointer-Based Strings 425

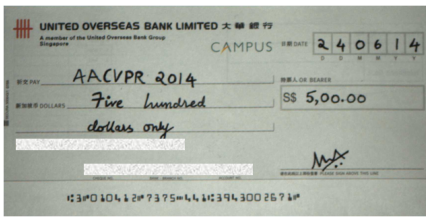
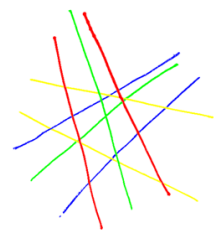
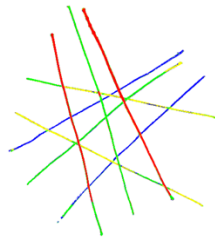
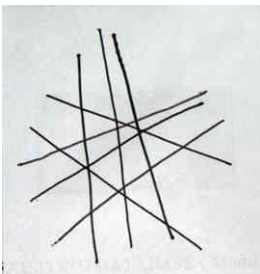
new imp
 (which is implicitly const) can be treated as a pointer and used in simple, the expression *

test ***
 element b[3]. In general, all subscripted array expressions can be an offset. In this case, pointer/offset notation was used with the inter. Note that the preceding expression does not modify the still points to the first element in the array.

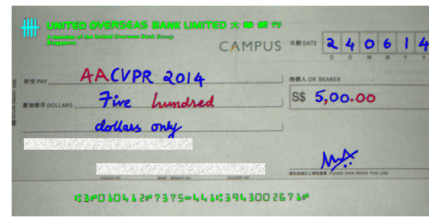
Pointers and Pointer-Based Strings 425

new imp
 (which is implicitly const) can be treated as a pointer and used in simple, the expression *

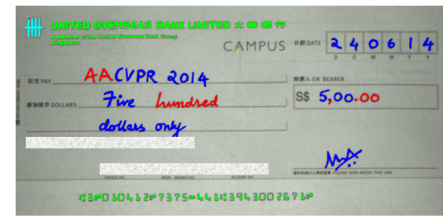
test ***
 element b[3]. In general, all subscripted array expressions can be an offset. In this case, pointer/offset notation was used with the inter. Note that the preceding expression does not modify the still points to the first element in the array.



(a)



(b)



(c)

Figure 9: Segmentation of ink strokes. a) Sample image. b) Segmentation result. c) Manually marked ground truth segmentation.

[16] S. Rusinkiewicz. A new change of variables for efficient brdf representation. In *Eurographics Rendering Workshop*, pages 11 – 22, 1998.

[17] B. Shi, P. Tan, Y. Matsushita, and K. Ikeuchi. A biquadratic reflectance model for radiometric image analysis. In *Proc. CVPR*, 2012.

[18] J. A. Siegel. *Ink Analysis*. Elsevier, second edition, 2013.

[19] M. M. Stark, J. Arvo, and B. Smits. Barycentric parameterizations for isotropic brdfs. *IEEE Trans. on Visualization and Computer Graphics*, 11(2):126–138, 2005.

[20] O. Wang, P. Gunawardane, S. Scher, and J. Davis. Material classification using brdf slices. In *Proc. CVPR*, pages 2805 –2811, 2009.

[21] C. Wu. *Visualsfm: A visual structure from motion system*. 2011.

[22] A. Yamashita, A. Kawarago, T. Kaneko, and K. T. Miura. Shape reconstruction and image restoration for non-flat surfaces of documents with a stereo vision system. pages 482–485. *Proc. ICPR*, 2004.

[23] W. Zhe and T. Ping. Calibrating photometric stereo by holistic reflectance symmetry analysis. In *Proc. CVPR*, 2013.